Wall-roughness induces asymptotic ultimate turbulence

Xiaojue Zhu,[1,*] Ruben A. Verschoof,[1,*] Dennis Bakhuis,[1] Sander G. Huisman,[2] Roberto Verzicco,[3,1] Chao Sun,[4,1,†] and Detlef Lohse[1,5,‡]

[1]*Physics of Fluids Group, MESA+ Institute and J. M. Burgers Centre for Fluid Dynamics, University of Twente, P.O. Box 217, 7500AE Enschede, The Netherlands*

[2]*Univ Lyon, Ens de Lyon, Univ Claude Bernard, CNRS, Laboratoire de Physique, F-69342 Lyon, France*

[3]*Dipartimento di Ingegneria Industriale, University of Rome "Tor Vergata", Via del Politecnico 1, Roma 00133, Italy*

[4]*Center for Combustion Energy and Department of Thermal Engineering, Tsinghua University, 100084 Beijing, China*

[5]*Max Planck Institute for Dynamics and Self-Organization, 37077 Göttingen, Germany*

(Dated: April 14, 2017)

Abstract

Turbulence is omnipresent in Nature and technology, governing the transport of heat, mass and momentum on multiple scales. For real-world applications of wall-bounded turbulence, the underlying surfaces are virtually always rough [1–3], yet characterizing the effects of wall-roughness for turbulence in closed systems remain an elusive challenge [4, 5]. By combining extensive experiments and numerical simulations of the paradigmatic Taylor-Couette system, the flow between two independently rotating concentric cylinders, we uncover the mechanism that causes the considerable enhancement of the overall transport properties by wall-roughness. If only one of the walls is rough, we reveal that the bulk velocity is slaved to the rough side, due to the much stronger coupling to that wall. If both walls are rough, the viscosity dependence is eliminated completely in the boundary layers and we thus achieve asymptotic ultimate turbulence, the upper limit of transport, whose existence had been predicted by R. Kraichnan in 1962 [6], in which the scalings laws can be extrapolated to arbitrarily large Reynolds numbers.

INTRODUCTION

While the vast majority of studies on wall-bounded turbulence assume smooth walls, flow boundaries are in general rough in engineering applications and the more in Nature, leading to a coupling of the small roughness scale with the much larger outer length scale of the turbulent flow. This holds for the atmospheric boundary layer over canopy or buildings, for geophysical flow, but also for many industrial flows such as pipe flow, for which the presumably most famous study on roughness was performed [7]. For excellent reviews on the effect of wall-roughness in turbulence we refer to Ref. [3] or textbooks such as Refs. [1, 2].

The disadvantage of pipe flow studies however is that the flow is not closed and that simultaneous measurements of local and global flow properties are difficult. This problem is overcome in Taylor-Couette (TC) flow [5], in which the overall torque τ to keep the cylinders at constant angular velocity is directly connected with the spatially averaged energy dissipation rate ϵ. This can be expressed in terms of the friction factor

$$c_f = \frac{\tau}{\ell\rho_f\nu^2(\mathrm{Re}_i - \eta\mathrm{Re}_o)^2} = \frac{\pi\eta}{(1-\eta)}\frac{\epsilon}{(U_i - \eta U_o)^3/(r_i + r_o)}. \tag{1}$$

Here $U_{i,o}$ are the velocities of the inner resp. outer cylinder, $r_{i,o}$ their radii, ν the kinematic viscosity (together defining the inner and outer Reynolds numbers $\mathrm{Re}_{i,o} = U_{i,o}d/\nu$), ρ_f the density of the fluid, ℓ the height of the TC cell, $d = r_o - r_i$ the gap width, and $\eta = r_i/r_o$ the ratio between outer and inner cylinder radius. The key question now is: how does the friction factor c_f depend on the (driving) Reynolds number Re_i and how does wall-roughness affect this relation?

Alternatively, the relation c_f can be expressed as a "Nusselt number" Nu_ω [8], where $\mathrm{Nu}_\omega = \tau/(2\pi\ell\rho_f J^\omega_{lam})$ with $J^\omega_{lam} = 2\nu r_i^2 r_o^2(\omega_i - \omega_o)/(r_o^2 - r_i^2)$ depending on the Taylor number $\mathrm{Ta} = \frac{1}{64}\frac{(1+\eta)^4}{\eta^2}d^2(r_i + r_o)^2(\omega_i - \omega_o)^2\nu^{-2}$ [5], with $\omega_{i,o}$ the angular velocity of the inner resp. outer cylinder. This notation $\mathrm{Nu}_\omega(\mathrm{Ta})$ stresses the analogy between TC flow and Rayleigh-Bénard flow (RB) [4, 9], the flow in a box heated from below and cooled from above, where the Nusselt number Nu (the dimensionless heat flux) depends on the Rayleigh number Ra (the dimensionless temperature difference). For that system Kraichnan [6] had postulated an ultimate scaling regime

$$\mathrm{Nu} \sim \mathrm{Ra}^{1/2}(\log \mathrm{Ra})^{-3/2} \tag{2}$$

(for fixed Prandtl number). In analogy, such an ultimate regime should also exist for TC flow, namely

$$\mathrm{Nu}_\omega \sim \mathrm{Ta}^{1/2}(\log \mathrm{Ta})^{-3/2}, \tag{3}$$

as worked out in Ref. [10]. In fact, in that reference slightly different log-dependences were derived, namely

$$\mathrm{Nu} \sim \mathrm{Ra}^{1/2}\mathcal{L}(\mathrm{Re}), \quad \text{and} \tag{4}$$

$$\mathrm{Nu}_\omega \sim \mathrm{Ta}^{1/2}\mathcal{L}(\mathrm{Re}), \tag{5}$$

where $\mathcal{L}(\mathrm{Re}(\mathrm{Ra}))$ resp. $\mathcal{L}(\mathrm{Re}(\mathrm{Ta}))$ are logarithmic dependences (see Methods and also Ref. [10]). Irrespective of whether one takes the logarithmic dependences (2) resp. (3) or (4) resp. (5), for smooth walls due to these log-corrections the *effective* scaling exponent for the largest experimentally achievable Rayleigh (Taylor) numbers is only around 0.38 and not 1/2, i.e., $\mathrm{Nu} \sim \mathrm{Ra}^{0.38}$ resp. $\mathrm{Nu}_\omega \sim \mathrm{Ta}^{0.38}$. This effective exponent 0.38 has indeed been observed in large Ra RB experiments [11, 12] and large Ta TC experiments [5, 13] and numerical simulations [5, 14]. The log-corrections, which are intimately connected with the logarithmic boundary layers [15], thus prevent the observation of the asymptotic ultimate regime exponent 1/2. This exponent has only been achieved in artificial configurations, such as numerical simulations of so-called "homogeneous turbulence" [16] with periodic boundary conditions and no boundary layers or experimental realisations thereof such as in ref. [17, 18]. The asymptotic exponent 1/2 in the Nu vs. Ra resp. Nu_ω vs. Ta scaling law corresponds to a friction factor c_f being *independent* on the Reynolds number. Vice versa, in the friction factor the logarithmic dependences of eqs. (2) to (5) are expressed in the so-called Prandtl-von Kármán skin friction law, i.e. $1/\sqrt{c_f} = a\log_{10}(\mathrm{Re}_i\sqrt{c_f}) + b$ [1, 2, 19], which can be obtained by assuming that the boundary layer profiles at each cylinder wall are logarithmic [20, 21]. Here a and b are fitting constants connected with the von Kármán constant κ.

How to get rid of the log-correction and to thus achieve asymptotic ultimate turbulence with a 1/2 power law or equivalently a Reynolds number independent friction factor? The path we will follow here is to introduce wall roughnnes. By combining direct numerical simulations (DNS) and experiments (EXP), we explore five decades of Ta to present conclusive evidence that the 1/2 power law can be realized, thus achieving the asymptotic ultimate regime. Moreover, we will give a theoretical justification for the findings based on measurements of the global and local flow structures and extend the analysis also to outer cylinder

rotation.

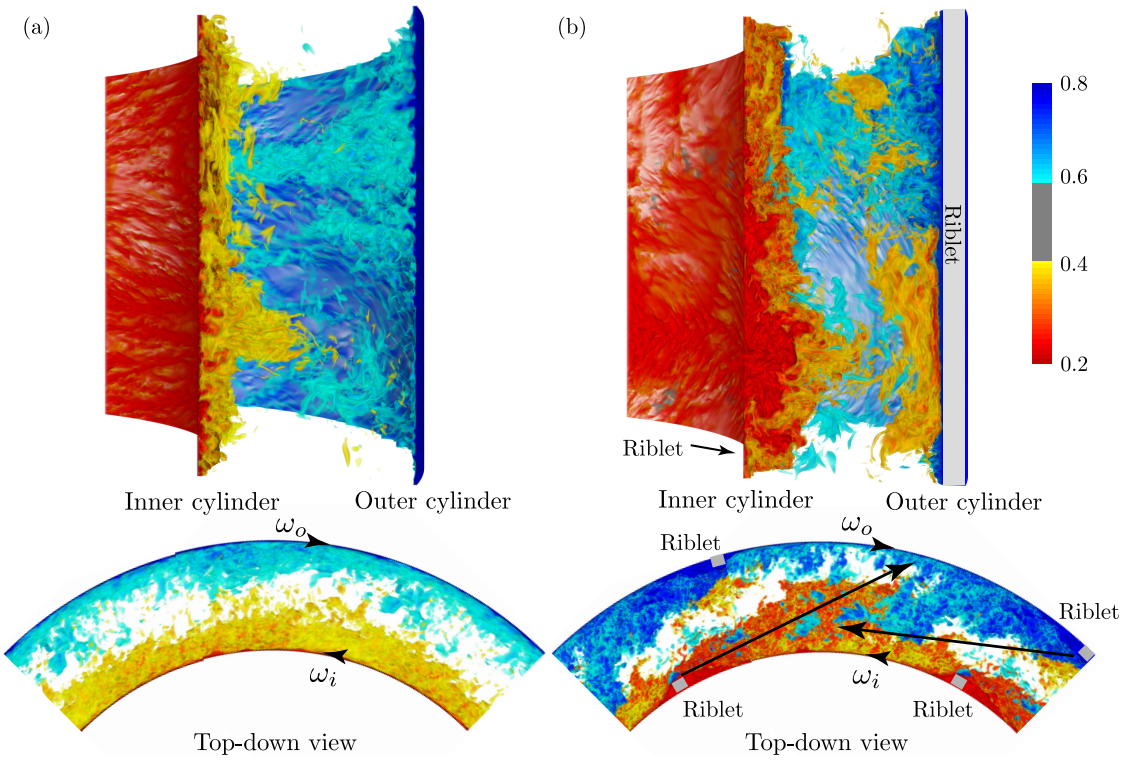

Figure 1: **Plume structures for smooth and rough Taylor-Couette turbulence.** Here the volume renderings of azimuthal velocity at $\mathrm{Ta} = 2.15 \times 10^9$ are shown, from numerical simulations. **a,** Both cylinders are smooth. We see that plumes are generated on both cylinders and form the structure of Taylor rolls. The plumes are concentrated in local regions and can not reach the other cylinder. **b,** Both cylinders are rough. Even in the rough case, Taylor rolls still exist. We see the plumes are also generated on top of the rough element and elongate to the other cylinder, and the arrows in the top-down views illustrate the directions of plumes. All plots share the same colormap.

Four cases will be considered: SS, SR, RS, and RR, where the first (second) letter specifies the configuration of the inner (outer) cylinder, which can be either rough (R) or smooth (S). In both DNS and EXP, the radius ratio between the two cylinders is $\eta = 0.716$. The cylinders were made rough by attaching six vertical ribs with a square cross-section over the entire height on none, both or either one of the cylinders (see Methods section). The roughness heights employed are much larger than the boundary layer thickness. To give the

reader an impression of the flow organization, typical flow structures of a smooth case and a rough case are shown in Figs. 1a,b, respectively.

GLOBAL SCALING RELATIONS

We first address the question of how roughness changes the global scaling relations. The global dimensionless torques, $\mathrm{Nu}_\omega \sim \mathrm{Ta}^\gamma$, for the four cases, with increasing Ta and fixed outer cylinder, are shown in Fig. 2a. Combining EXPs and DNSs, the range of Taylor number studied here extends five decades. Similar to what has been shown in various studies recently [11, 14, 21–24], for the SS case, an effective scaling of $\mathrm{Nu}_\omega \sim \mathrm{Ta}^{0.38\pm0.02}$ is observed in the DNS, corresponding to the ultimate regime with logarithmic corrections [6, 10]. Very similar scaling exponent $\mathrm{Nu}_\omega \sim \mathrm{Ta}^{0.39\pm0.01}$ is found in EXP, demonstrating the excellent agreement between DNS and EXP. Dramatic enhancements of the torques are clearly observed with the introduction of wall-roughness, resulting in the transition of Nu_ω from $\mathcal{O}(10^2)$ to $\mathcal{O}(10^3)$. Specifically, when only a single cylinder is rough, the logarithmic corrections reduce and the scaling exponents marginally increase, implying the scaling in the flow is dominated by the single smooth wall. For the RR case, best fits of $\mathrm{Nu}_\omega \sim \mathrm{Ta}^{0.50\pm0.02}$ are obtained both numerically and experimentally, suggesting that the logarithmic corrections are canceled and the asymptotic ultimate scaling 1/2 is seen. The compensated plots of insets of $\mathrm{Nu}_\omega \,/\, \mathrm{Ta}^\gamma$ show the robustness and the quality of the scalings.

When expressing the relation between the global transport properties and the driving force in terms of the Reynolds number dependence of the friction factor c_f we obtain Fig. 2b. For the SS case, the fitting parameters a and b yield a von Kármán constant $\kappa = 0.44 \pm 0.01$, which is slightly larger than the standard value of 0.41 due to the curvature effect [15, 20, 25]. This agrees very well with the previous measurements on TC with smooth walls [26]. For the RR case, in both DNS and EXP, the friction factor c_f is found to be independent on Re_i, namely $c_f = 0.29$ in the DNS and $c_f = 0.23$ in the EXP. The discrepancy is caused by the implementation of different heights of riblet in DNS (10% of the cylinders gap width) and EXP (7.5% of the cylinders gap width). If we use the same 10% gap width riblet in DNS, we find $c_f = 0.23$. The results here are consistent with the asymptotic ultimate regime scaling 1/2 for Nu_ω and indicate that the Prandtl-von Kármán log-law of the wall [1] with wall-roughness is also independent of Re_i [7], which has been verified recently for Taylor-

Couette flow [27]. Note that in pipe flow, the same Reynolds number independent friction factor with wall-roughness is observed [1, 2]. For the RS and SR cases, one boundary is rough and the other is smooth such that the friction law lies in between RR and SS lines.

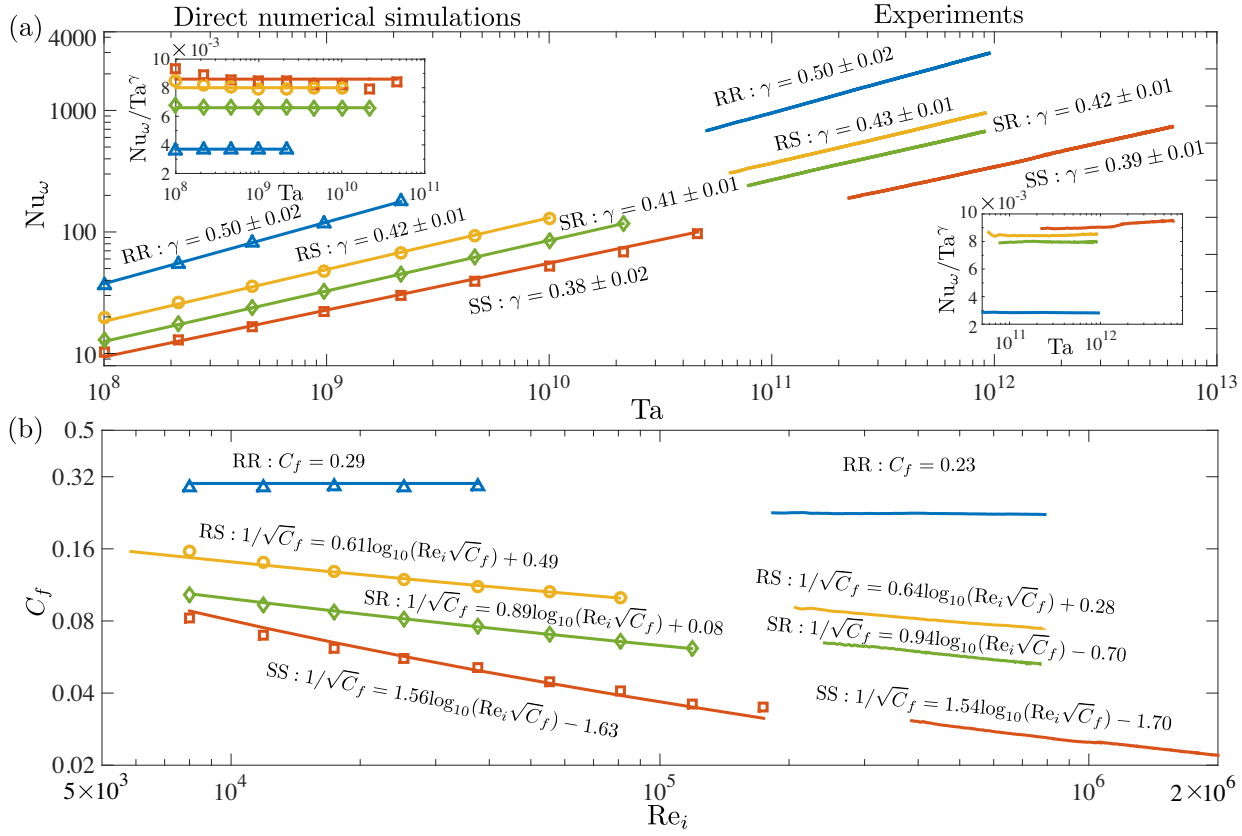

Figure 2: **Global torque and friction factor scalings.** **a,** The dimensionless torque as a function of Taylor number Ta: DNS (left part), and experiments (right part). Four cases are shown: (SS) both cylinders rough; (SR) smooth inner, rough outer; (RS) rough inner, smooth outer; and (RR) both cylinders rough, with the exponent γ in the power law relation $\mathrm{Nu}_\omega \sim \mathrm{Ta}^\gamma$ shown for every case. The inset depicts the compensated plots $\mathrm{Nu}_\omega \,/\, \mathrm{Ta}^\gamma$, showing the quality of the scaling. **b,** The friction factor c_f as a function of the inner cylinder Reynolds number Re_i: DNS (left part), and experiments (right part). The lines show the best fits of the Prandtl friction law $1/\sqrt{c_f} = a\log_{10}(\mathrm{Re}_i\sqrt{c_f}) + b$, with all prefactors shown in the figures. For RR case, Re_i independent friction factors ($c_f = 0.29$ (DNS) and $c_f = 0.23$ (EXP)) are revealed.

We now interpret the torque scalings through an extension of the Grossmann-Lohse (GL) theory [10], by accounting for Prandtl-von Kármán log-law of the wall [1] in the presence

of roughness. To show how this theory works, we take the example of only inner cylinder rotation. For a smooth wall, the energy dissipation rate in the log region scales with $\epsilon_u d^4/\nu^3 \sim \mathrm{Re}_i^3 (u_\tau/U)^3 \ln(\mathrm{Re}_i\, u_\tau/U)$, which stems from the integration of the Prandtl-von Kármán log-law of the wall, where u_τ is the friction velocity and U the velocity of inner cylinder. The log term in the law is dependent on Re_i, which is the origin of the logarithmic correction term $\mathcal{L}(\mathrm{Re}) = (u_\tau/U)^3 \ln(\mathrm{Re}_i\, u_\tau/U)$ besides the asymptotic ultimate regime scaling $\epsilon_u d^4/\nu^3 \sim \mathrm{Re}_i^3$ and thus decreases the effective scaling exponent. However, with roughness, the log term in the law of the wall is independent of Re_i [27], which correspondingly renders this correction *constant*. Therefore, by linking the energy dissipation rate ϵ_u, Reynolds number Re_i with the dimensionless torque Nu_ω and driving force Ta [8], the effect of logarithmic term on the scaling vanishes and asymptotic ultimate scaling $\mathrm{Nu}_\omega \sim \mathrm{Ta}^{1/2}$ emerges; see Methods for details.

In a TC system, the inner and outer cylinders can rotate independently, resulting in the rotation ratio between the two cylinders $a = -\omega_o/\omega_i$ as another important parameter. Also with rough walls the $\mathrm{Nu}_\omega \sim \mathrm{Ta}^\gamma$ scalings are independent of rotation ratio, the same for the smooth wall cases [22]. For long, it has been known that inner cylinder rotation has a destabilizing effect on the flow, whereas outer cylinder rotation has a stabilizing effect [28]. For TC flow with smooth walls, it was found that the optimal transport rotation ratio a_{opt} between the two cylinders, where the torque reaches the maximum for a specific driving Ta, is around 0.36 [29, 30] instead of zero. Later it was verified that this is attributed to the existence of the strong Taylor rolls between the counter-rotating cylinders when $a < a_{opt}$. Only for strong enough counter-rotation ($a > a_{opt}$) does the stabilization through the counter-rotating outer cylinder take over [31]. Here, we focus on whether this optimal transport rotation ratio shifts or stays the same in the presence of roughness. The results are shown in figure 3. We find that when either one of the cylinders is rough, the effect of that rough cylinder is enhanced.

In the SR case, little outer cylinder rotation is necessary to stabilize the flow efficiently with the help of the roughness elements. In contrast, a rough inner cylinder is much more effective to enhance the momentum transport. The optimal transport peak for the RS case occurs at larger rotation ratios, as a high outer cylinder rotation is needed to suppress turbulence originating from the inner cylinder. In this case the stabilizing effect of the smooth outer cylinder becomes inefficient. In the RR case, the effects of the inner cylinder

and outer cylinder are balanced in a similar way as in the SS case, resulting in the similar values of a_{opt} found in the SS case. At optimal rotation ratio a_{opt}, the enhanced shear is caused by Taylor rolls [14, 29, 30, 32]. This indicates that even with the presence of roughness, Taylor rolls still exist, as visible in Fig. 1.

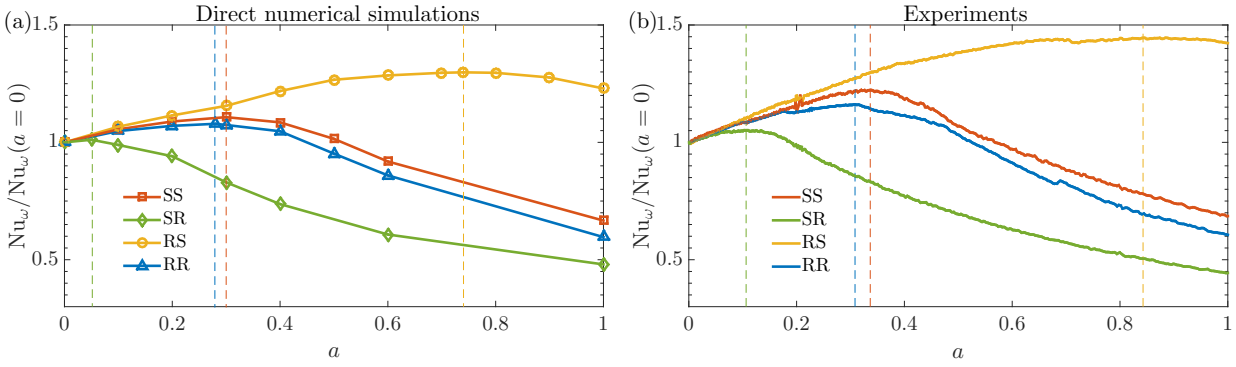

Figure 3: **Optimal transport peak** Nu_ω as a function of a for constant driving strength, normalized by its value for $a = 0$. **a,** DNSs with $\mathrm{Ta} = 1 \times 10^9$. The optimal transport peaks are located at $a_{opt,SS} = 0.30$, $a_{opt,SR} = 0.06$, $a_{opt,RS} = 0.74$ and $a_{opt,RR} = 0.28$. **b,** Experiments with $\mathrm{Ta} = 4 \times 10^{11}$. The optimal transport peaks for the 4 cases are located at $a_{opt,SS} = 0.34$, $a_{opt,SR} = 0.11$, $a_{opt,RS} = 0.84$ and $a_{opt,RR} = 0.31$. All optimal transport peaks are indicated by the dashed lines.

LOCAL FLOW ORGANIZATION AND PROFILES

Till now, we have focused on the global transport properties, however, the details of boundary layer-bulk interaction, and in particular how the local scalings affect the global ones, are still unknown. To verify the theory mentioned before, we split the mean energy dissipation rate from our DNS data into boundary layer and bulk contributions, following the GL approach [33, 34]. In Fig. 4(a), the local energy dissipation rates at mid-gap $\epsilon_{u,c}$ are shown as a function of Ta (only inner cylinder rotation). It is clear that no matter whether the wall is smooth or rough, the bulk energy dissipation rate follows $\epsilon_{u,c} \sim \mathrm{Ta}^{3/2} \sim \mathrm{Re}_i^3$, which corresponds to the asymptotic ultimate regime without any logarithmic correction. In analogy, for RB turbulence, the same scaling exponent $\epsilon_{u,c} \sim \mathrm{Ra}^{3/2}$ was reported in Refs. [35, 36]. Therefore, the crucial element determining the overall scaling is the dissipation

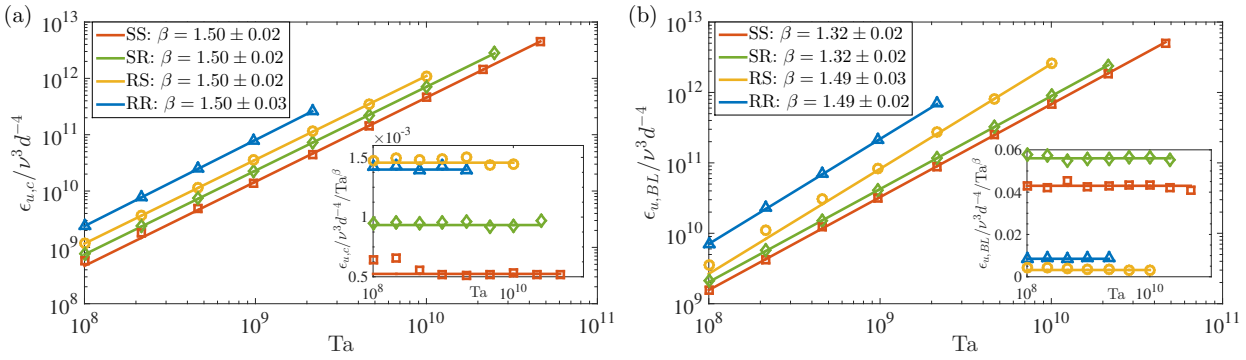

Figure 4: **Local energy dissipation rate from simulations.** Local energy dissipation rate in the bulk $\epsilon_{u,c}$ (at the center of the gap, averaged over the height) and in the inner cylinder boundary layer $\epsilon_{u,BL}$ (averaged in the range of wall distance zero to the point of maximum root mean square of azimuthal velocity) as a function of Ta. The symbols are the same as in Fig. 2. The lines show the best fits of them. **a,** The bulk energy dissipation rate follows $\epsilon_{u,c} \sim \mathrm{Ta}^{1.50} \sim Re_i^3$, irrespective of whether the wall is smooth or rough. **b,** The boundary layer dissipation rate follows $\epsilon_{u,BL} \sim \mathrm{Ta}^{1.32}$ for the cases with smooth walls while it scales with $\epsilon_{u,BL} \sim \mathrm{Ta}^{1.50}$ for cases with rough walls.

rate in the boundary layer. To further confirm this, we show the local energy dissipation rates of the boundary layer $\epsilon_{u,BL}$ (averaged in the range of wall distance zero to the point of maximum root mean square of azimuthal velocity) in Fig. 4 (b). For the case with smooth walls, we find $\epsilon_{u,BL} \sim \mathrm{Ta}^{1.32}$ because of the Re_i dependent velocity profile, while for the boundary layers at rough walls we have $\epsilon_{u,BL} \sim \mathrm{Ta}^{3/2}$ because, as shown above, roughness cancels out the Re_i dependence and thus restores the asymptotic ultimate regime scaling. The competition between the boundary layer and bulk ultimately determines the global scalings.

From another point of view, roughness blocks the flow. Therefore, the main contribution to the torque comes from the pressure differences between the side surfaces of rough elements, rather than viscous forces. With roughness, we expect the shear rate close to the rough wall to decrease significantly, compared with the smooth case. This is clearly shown in Fig. 5. With smooth cylinders, the normalized velocity profiles are characterized by a bulk region, in which the velocity is relatively constant ($U_\theta = 0.45 r_i \omega_i$). When a single cylinder is rough, the bulk velocity is completely dominated by the velocity of the rough cylinder, or in other words, bulk is enslaved by the rough wall. In the RR case, although the impact of roughness

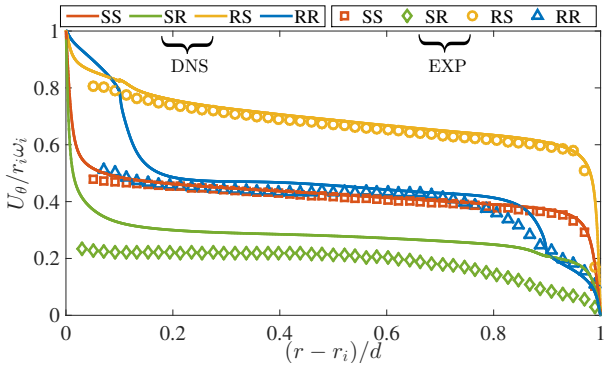

Figure 5: **Mean velocity profiles.** Normalized azimuthal velocity $U_\theta(r)/(r_i\omega_i)$ profiles as a function of the normalized radius $(r-r_i)/d$ for only inner cylinder rotation. Experimental and numerical data are shown in the same figure. EXP: $\mathrm{Re}_i = 5\times10^5$ and DNS: $\mathrm{Re}_i = 3.74\times10^4$. The experimental results were obtained using PIV.

to the bulk flow balances, because that the torque is still dominated by pressure forces, the shear rate at the rough cylinder is also smaller as compared with the smooth case. The implication is that with roughness, a larger fraction of energy dissipates in the bulk, and thus the system is more bulk dominant. As mentioned before, the bulk energy dissipation rate follows $\epsilon_{u,c} \sim \mathrm{Ta}^{3/2}$, which implies the asymptotic ultimate regime. The more bulk is dominant, the closer the system reaches the ultimate regime without any logarithmic correction. This is indeed verified by the flow structure in Fig. 1, where for the rough case, the plumes shedding from the roughness elements on one wall elongate towards the other wall and push more energy dissipation in the bulk compared to the smooth case.

CONCLUSIONS AND OUTLOOK

Despite that in recent years various studies have been performed on turbulence with wall-roughness in closed systems, the results are highly scattered on the power law exponents between the transport and the driving forces [37–42], i.e. there is no consensus on whether asymptotic ultimate turbulence 1/2 power law, a concept that was postulated 50 years ago by R. Kraichnan [6], can be achieved or not [4]. In contrast, here with both strong experimental and numerical evidence, we demonstrate that the asymptotic ultimate regime exponent 1/2, the upper limit of transport, can be realized with the implementation of wall-roughness. The mechanism is that wall-exponent roughness eliminates the Reynolds number dependence of

transport inside the boundary layer, thus helps to attain the asymptotic ultimate regime. The insights gained from this study provides valuable guidance for wall-bounded turbulence with wall-roughness in the ultimate regime in general, which is useful for a wide range of applications in industrial, geophysical, meteorological and oceanographical flows.

METHODS

Experimental methods

Experimental apparatus

The experiments were performed in the Twente Turbulent Taylor-Couette facility (T^3C) [43], consisting of two independently rotating concentric cylinders. The setup has an inner cylinder with a radius of $r_i = 200$ mm and an outer cylinder with a radius of $r_o = 279.4$ mm, resulting in a radius ratio of $\eta = r_i/r_o = 0.716$ and a gap width of $d = r_o - r_i = 79$ mm. The gap is filled with water with a temperature of T $\approx 20°$C. In this work, the inner and outer cylinder rotate up to $\omega_i/2\pi = 7.5$ Hz and $\omega_o/2\pi = 5$ Hz, respectively, resulting in Reynolds numbers up to $\mathrm{Re}_i = \omega_i r_i d/\nu = 7.5 \times 10^5$ and $\mathrm{Re}_o = \omega_o r_o d/\nu = 7 \times 10^5$. The cylinders have a height of $L = 927$ mm, resulting in an aspect ratio of $\Gamma = L/(r_o - r_i) = 11.7$. The end plates rotate with the outer cylinder. The cylinders were made rough by attaching 6 vertical strips with a square cross-section (6×6 mm, i.e. 7.5% of the gap width) over the entire height on none, both or either one of the cylinders, similar as in ref. [41, 44] (Fig. 6). The roughness height is much larger than the boundary layer thickness [20].

Torque measurements

The torque is measured with a co-axial torque transducer (Honeywell 2404-5K, maximum capacity of 565 Nm), located inside the inner cylinder, to avoid measurement errors due to seals- and bearing friction, as shown in figure 6. In previous studies using this setup, the inner cylinder consisted of 3 different compartments, in which torque was measured in the middle section to exclude end plate effects [22, 29, 31]. Here, we measure over the entire height of the cylinder, which accounts for the slightly different results for the SS case as compared to these studies.

Velocity measurements

Planar particle image velocimetry (PIV) measurements were performed in the $\theta - r$ plane at mid-height ($z = L/2$). We used a high-resolution sCMOS camera (pco.edge camera with

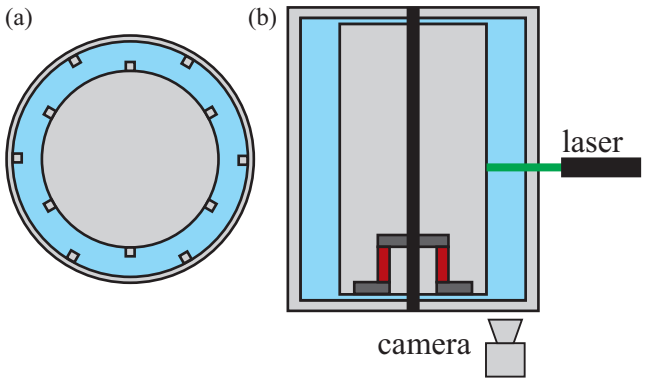

Figure 6: **Experimental setup** (a) Schematic of the top view of both the experimental and numerical setup for the (RR) case, i.e. both cylinders rough. The six ribs (not to scale), which are perpendicular to the axis of rotation, have a square cross section and extend over the entire height of the cylinders. Their size is 7.5% and 10% of the gap width for the experiments and DNSs, respectively (b) Vertical cross-section of the experimental setup, showing the position of the torque sensor and the PIV setup. For the PIV measurements, the laser illuminates the horizontal (r, θ) plane at mid-height, $z = L/2$, see the Methods section.

2560 px $\times$ 2160 px resolution), which was operated in double frame mode, as depicted in fig. 6. We record images through transparent windows in the bottom plate. The flow was illuminated from the side with a pulsed laser (532 nm Quantel Evergreen 145 Nd:YLF). The water was seeded with 20 μm fluorescent polymer particles (PMMA-RhB-10 by Dantec). The sheet thickness was approximately 1 mm. The PIV measurements were processed to give the averaged azimuthal velocity as a function of the radius $\langle u_\theta(r)\rangle_\theta$.

Numerical methods

The motion of the fluid is governed by the incompressible Navier-Stokes equations in the frame co-rotating with the outer cylinder

$$\frac{\partial \mathbf{u}}{\partial t} + \mathbf{u}\cdot\nabla\mathbf{u} = -\nabla p + \frac{f(\eta)}{\mathrm{Ta}^{1/2}}\nabla^2\mathbf{u} - \mathrm{Ro}^{-1}\,\mathbf{e}_z\times\mathbf{u}, \tag{6}$$

$$\nabla\cdot\mathbf{u} = 0, \tag{7}$$

where $\mathbf{u}$ and p are the fluid velocity and pressure, respectively. $f(\eta)$ is a geometrical factor which is in the form

$$f(\eta) = \frac{(1+\eta)^3}{8\eta^2}. \tag{8}$$

Ta is the Taylor number and Ro the Rossby number which characterizes the strength of the driving force. The rotation ratio $a = -\omega_o/\omega_i$ is interchangeable with Rossby number through

$$\mathrm{Ro}^{-1} = \frac{2\omega_o d}{|\omega_i - \omega_0| r_i} = -2\frac{1-\eta}{\eta}\frac{a}{|1+a|}. \tag{9}$$

The inner cylinder Reynolds number $\mathrm{Re}_i = r_i\omega d/\nu$ and outer cylinder Reynolds number $\mathrm{Re}_o = r_o\omega d/\nu$ are associated with Ta and Ro through

$$\mathrm{Re}_i = \frac{\mathrm{Ta}^{1/2}}{f(\eta)}\left(1 + \frac{\eta\,\mathrm{Ro}^{-1}}{2(1-\eta)}\right) \tag{10}$$

and

$$\mathrm{Re}_o = \frac{\mathrm{Ro}^{-1}\,\mathrm{Ta}^{1/2}}{2f(\eta)(1-\eta)}. \tag{11}$$

The governing equations are solved using an energy conserving second-order finite-difference code [45], in combination with an immersed-boundary method [46, 47] to deal with the roughness. To achieve high performance computation, a two-dimensional MPI decomposition technique (MPI-pencil) [48] is adopted. Weak and strong scaling tests show the linear behaviour of the code up to 64K cores. The code has been extensively validated and used for TC flow with smooth [14, 21, 49] and rough [27, 50] walls. The axial direction is periodic and thus the end plate effects [51] are eliminated. The radius ratio is chosen as $\eta = 0.716$. The aspect ratio of the computational domain $\Gamma = L/d$, where L is the axial periodicity length, is taken as $\Gamma = 2.09$. When both walls are roughened, the inner and outer cylinder surfaces have six vertical ribs of square cross section (edge width $h = 0.1d$), respectively. The riblets are equi-distributed in the azimuthal direction, similar to the experimental implementation. A rotational symmetry of order $n_{sym} = 6$ is imposed to achieve a minimum azimuthal extent. The computation box is tested to be large enough to capture the sign changes of the azimuthal velocity autocorrelation at the mid-gap, as suggested as a criterion for the box size [49]. Besides, the appropriate number of grid points is chosen to make sure that enough resolution has been employed [14, 21]. E.g. at $\mathrm{Ta} = 2.15 \times 10^9$ for the RR case, $3072 \times 1536 \times 1536$ grid points are used.

Extention of Grossmann-Lohse theory with wall-roughness

To explain the asymptotic ultimate scaling 1/2 found in this manuscript, here we first recall the origin of the logarithmic correction. We take the case of only inner rotation as an example. According to the Grossmann-Lohse (GL) theory [10], the local dissipation rate in the turbulent boundary layer [52] is given by

$$\epsilon_u(z) = u_\tau^3/(\kappa z), \tag{12}$$

where $u_\tau = \sqrt{\tau/(2\rho\pi r^2 L)}$ is the friction velocity, with ρ is the fluid density, κ the von Kármán constant, r can be either the inner cylinder radius r_i or the outer one r_o, and z is the distance from the wall. u_τ is connected with the inner cylinder velocity $U = r_i\omega_i$ through the law of the wall [1], which is shown for TC turbulence in Refs. [20, 21] to obey

$$\frac{u_\tau}{U} = \frac{\kappa}{\ln(\mathrm{Re}_i\, u_\tau/U/B)}. \tag{13}$$

Re_i is the inner cylinder Reynolds number and which for pure inner cylinder rotation can be related to Ta through the expression $\mathrm{Ta} = \frac{(1+\eta)^6}{64\eta^4}\,\mathrm{Re}_i^2$, B is a constant depending on the system geometry. By averaging the local dissipation rate along the radius, we can estimate the mean dissipation rate as

$$\begin{aligned}
\epsilon_{u,m} &\sim \frac{1}{d/2}\int_0^{d/2} \epsilon_u(z)dz \\
&= \nu^3 d^{-4}\,\mathrm{Re}_i^3\, L(\mathrm{Re}_i) \\
&= \nu^3 d^{-4}\,\mathrm{Re}_i^3 \left(\frac{u_\tau}{U}\right)^3 \frac{2}{\kappa}\ln\left(\mathrm{Re}_i\,\frac{u_\tau}{U}\frac{1}{2}\right).
\end{aligned} \tag{14}$$

Here we assume that logarithmic boundary layer extends from the wall to the mid-gap. Usually how far the log-layer extends depends on Re_i and can be a small fraction of the gap width, but still for both TC and pipe flows, taking the half gap width or radius is a reasonable approximation to derive the friction laws [1, 2, 23, 26]. The term $\mathcal{L}(\mathrm{Re}_i) = (u_\tau/U)^3\ln(\mathrm{Re}_i\, u_\tau/U)$, depending on Re_i, is the logarithmic correction [10]. Using the well known exact relation between $\epsilon_{u,m}$ and Nu_ω, namely $\epsilon_{u,m} = \nu^3 d^{-4}\,\mathrm{Ta}(\mathrm{Nu}_\omega - 1)\left(\frac{\sqrt{\eta}}{(1+\eta)/2}\right)^8$ [8] and $\mathrm{Ta} \sim \mathrm{Re}_i^2$, one obtains

$$\frac{\epsilon_{u,m}}{\nu^3 d^{-4}} \sim \mathrm{Re}_i^3\,\mathcal{L}(\mathrm{Re}_i) \text{ and } \mathrm{Nu}_\omega \sim \mathrm{Ta}^{1/2}\ \mathcal{L}(\mathrm{Re}_i). \tag{15}$$

with the logarithmic correction $\mathcal{L}(\mathrm{Re}_i)$ for both dissipation rate and torque scalings. It leads to a less steep increase of ϵ_u with increasing Re_i than in the Kolmogorov bulk which scales as

Re_i^3, and hence decreases the torque scaling between Nu_ω and Ta from asymptotic ultimate scaling 1/2 to the effective scaling 0.38 [10, 11, 22], as mentioned before.

With both walls roughened, the log-law in the fully rough regime ($u_\tau h/\nu > 70$ [1]; all our rough cases are in this regime) becomes

$$\frac{u_\tau}{U} = \frac{\kappa}{\ln(d/h/B)}, \tag{16}$$

as shown for turbulent TC flow with one rough boundary layer in Ref. [27]. The momentum transfer between the wall and the fluid is accomplished by the shear, which in the fully rough regime occurs predominantly by the pressure forces on the side surfaces of the rough elements, rather than by viscous forces [2]. That in the ultimate regime the kinematic viscosity ν is an irrelevant parameter, is reflected in the velocity profile (Eq. (16)) being *independent* of Re_i. Replacing the velocity profile from the smooth one to the rough one in Eqs. (12, 13, 14), remarkably we find that the logarithmic correction term for $\epsilon_{u,m}$ turns into a *constant* and thus its effect on the scaling exponent vanishes. The mean dissipation rate and torque thus now scale as

$$\frac{\epsilon_{u,m}}{\nu^3 d^{-4}} \sim \mathrm{Re}_i^3 \ \text{ and } \ \mathrm{Nu}_\omega \sim \mathrm{Ta}^{1/2}, \tag{17}$$

which explains the asymptotic ultimate regime scaling seen in Fig. 2 for the RR case. In the RS case, the boundary layer at smooth wall depends on Re_i while boundary layer at rough wall is independent of it, the logarithmic correction is reduced but not totally canceled.

---

* These authors contributed equally to this work

† Electronic address: chaosun@tsinghua.edu.cn

‡ Electronic address: d.lohse@utwente.nl

[1] H. Schlichting and K. Gersten, Boundary layer theory, 8th ed. (Springer Verlag, Berlin, 2000).

[2] S. B. Pope, Turbulent Flow (Cambridge University Press, Cambridge, 2000).

[3] J. Jimenez, Turbulent flows of rough walls, Ann. Rev. Fluid Mech. **36**, 173 (2004).

[4] G. Ahlers, S. Grossmann, and D. Lohse, Heat transfer and large scale dynamics in turbulent Rayleigh-Bénard convection, Rev. Mod. Phys. **81**, 503 (2009).

[5] S. Grossmann, D. Lohse, and C. Sun, High Reynolds number Taylor-Couette turbulence, Ann. Rev. Fluid Mech **48**, 53 (2016).

[6] R. H. Kraichnan, Turbulent thermal convection at arbritrary Prandtl number, Phys. Fluids **5**, 1374 (1962).

[7] J. Nikuradse, Strömungsgesetze in rauhen Rohren, Forschungsheft Arb. Ing.-Wes. **361**, (1933).

[8] B. Eckhardt, S. Grossmann, and D. Lohse, Torque scaling in turbulent Taylor-Couette flow between independently rotating cylinders, J. Fluid Mech. **581**, 221 (2007).

[9] D. Lohse and K.-Q. Xia, Small-scale properties of turbulent Rayleigh-Bénard convection, Ann. Rev. Fluid Mech. **42**, 335 (2010).

[10] S. Grossmann and D. Lohse, Multiple scaling in the ultimate regime of thermal convection, Phys. Fluids **23**, 045108 (2011).

[11] X. He, D. Funfschilling, H. Nobach, E. Bodenschatz, and G. Ahlers, Transition to the ultimate state of turbulent Rayleigh-Bénard convection, Phys. Rev. Lett. **108**, 024502 (2012).

[12] X. He, D. Funfschilling, E. Bodenschatz, and G. Ahlers, Heat transport by turbulent Rayleigh-Bénard convection for $Pr = 0.8$ and $4 \times 10^{11} < Ra < 2 \times 10^{14}$: ultimate-state transition for aspect ratio $\Gamma = 1.00$, New J. Phys.. **14**, 063030 (2012).

[13] S. G. Huisman, D. P. M. van Gils, S. Grossmann, C. Sun, and D. Lohse, Ultimate turbulent Taylor-Couette flow, Phys. Rev. Lett. **108**, 024501 (2012).

[14] R. Ostilla-Mónico, E. P. van der Poel, R. Verzicco, S. Grossmann, and D. Lohse, Exploring the phase diagram of fully turbulent Taylor-Couette flow, J. Fluid Mech. **761**, 1 (2014).

[15] R. Ostilla-Mónico, R. Verzicco, S. Grossmann, and D. Lohse, The near-wall region of highly turbulent Taylor-Couette flow, J. Fluid Mech. **788**, 95 (2016).

[16] D. Lohse and F. Toschi, The ultimate state of thermal convection, Phys. Rev. Lett. **90**, 034502 (2003).

[17] M. Gibert, H. Pabiou, F. Chilla, and B. Castaing, High-Rayleigh-number convection in a vertical channel, Phys. Rev. Lett. **96**, 084501 (2006).

[18] M. Cholemari and J. Arakeri, Axially homogeneous, zero mean flow buoyancy-driven turbulence in a vertical pipe, J. Fluid Mech. **621**, 69 (2009).

[19] T. von Karman, Uber laminare und turbulente Reibung, Z. angew. Math. Mech. **1**, 233 (1921).

[20] S. G. Huisman, S. Scharnowski, C. Cierpka, C. Kähler, D. Lohse, and C. Sun, Logarithmic boundary layers in strong Taylor-Couette turbulence, Phys. Rev. Lett. **110**, 264501 (2013).

[21] R. Ostilla-Mónico, E. P. van der Poel, R. Verzicco, S. Grossmann, and D. Lohse, Boundary layer dynamics at the transition between the classical and the ultimate regime

of Taylor-Couette flow, Phys. Fluids **26**, 015114 (2014).

[22] D. P. M. van Gils, S. G. Huisman, G. W. Bruggert, C. Sun, and D. Lohse, Torque scaling in turbulent Taylor-Couette flow with co- and counter-rotating cylinders, Phys. Rev. Lett. **106**, 024502 (2011).

[23] D. P. Lathrop, J. Fineberg, and H. S. Swinney, Turbulent flow between concentric rotating cylinders at large Reynolds numbers, Phys. Rev. Lett. **68**, 1515 (1992).

[24] H. J. Brauckmann and B. Eckhardt, Direct numerical simulations of local and global torque in Taylor-Couette flow up to Re = 30 000, J. Fluid Mech. **718**, 398 (2013).

[25] H. J. Brauckmann and B. Eckhardt, Intermittent boundary layers and torque maxima in Taylor-Couette flow, Phys. Rev. E **87**, 033004 (2013).

[26] G. S. Lewis and H. L. Swinney, Velocity structure functions, scaling, and transitions in high-Reynolds-number Couette-Taylor flow, Phys. Rev. E **59**, 5457 (1999).

[27] X. Zhu, R. Verzicco, and D. Lohse, Disentangling the origins of torque enhancement through wall roughness in Taylor-Couette turbulence, J. Fluid Mech. **812**, 279 (2017).

[28] G. I. Taylor, Stability of a viscous liquid contained between two rotating cylinders, Phil. Trans. R. Soc. A **223**, 289 (1923).

[29] S. G. Huisman, R. C. A. van der Veen, C. Sun, and D. Lohse, Multiple states in highly turbulent Taylor-Couette flow, Nat. Commun. **5**, 3820 (2014).

[30] R. C. A. van der Veen, S. G. Huisman, O.-Y. Dung, H.-L. Tang, C. Sun, and D. Lohse, Exploring the phase space of multiple states in highly turbulent Taylor-Couette flow, Phys. Rev. Fluids **1**, 024401 (2016).

[31] D. P. M. van Gils, S. G. Huisman, S. Grossmann, C. Sun, and D. Lohse, Optimal Taylor-Couette turbulence, J. Fluid Mech. **706**, 118 (2012).

[32] S. Maretzke, B. Hof, and M. Avila, Transient growth in linearly stable Taylor-Couette flows, J. Fluid Mech. **742**, 254 (2014).

[33] S. Grossmann and D. Lohse, Scaling in thermal convection: A unifying view, J. Fluid. Mech. **407**, 27 (2000).

[34] S. Grossmann and D. Lohse, Thermal convection for large Prandtl number, Phys. Rev. Lett. **86**, 3316 (2001).

[35] X. D. Shang, P. Tong, and K.-Q. Xia, Scaling of the local convective heat flux in turbulent Rayleigh-Bénard convection, Phys. Rev. Lett. **100**, 244503 (2008).

[36] R. Ni, S.-D. Huang, and K.-Q. Xia, Local Energy Dissipation Rate Balances Local Heat Flux in the Center of Turbulent Thermal Convection, Phys. Rev. Lett. **107**, 174503 (2011).

[37] S. Ciliberto and C. Laroche, Random roughness of boundary increases the turbulent convection scaling exponent, Phys. Rev. Lett. **82**, 3998 (1999).

[38] Y. Shen, P. Tong, and K.-Q. Xia, Turbulent convection over rough surfaces, Phys. Rev. Lett. **76**, 908 (1996).

[39] Y. B. Du and P. Tong, Turbulent thermal convection in a cell with ordered rough boundaries, J. Fluid Mech. **407**, 57 (2000).

[40] P. E. Roche, B. Castaing, B. Chabaud, and B. Hebral, Observation of the 1/2 power law in Rayleigh-Bénard convection, Phys. Rev. E **63**, 045303 (2001).

[41] T. H. van den Berg, C. Doering, D. Lohse, and D. Lathrop, Smooth and rough boundaries in turbulent Taylor-Couette flow, Phys. Rev. E **68**, 036307 (2003).

[42] J. C. Tisserand, M. Creyssels, Y. Gasteuil, H. Pabiou, M. Gibert, B. Castaing, and F. Chilla, Comparison between rough and smooth plates within the same Rayleigh-Benard cell, Phys. Fluids **23**, 015105 (2011).

[43] D. P. M. van Gils, G. W. Bruggert, D. P. Lathrop, C. Sun, and D. Lohse, The Twente turbulent Taylor-Couette (T^3C) facility: strongly turbulent (multi-phase) flow between independently rotating cylinders, Rev. Sci. Instr. **82**, 025105 (2011).

[44] O. Cadot, Y. Couder, A. Daerr, S. Douady, and A. Tsinober, Energy injection in closed turbulent flows: Stirring through boundary layers versus inertial stirring, Phys. Rev. E **56**, 427 (1997).

[45] R. Verzicco and P. Orlandi, A finite-difference scheme for three-dimensional incompressible flow in cylindrical coordinates, J. Comput. Phys. **123**, 402 (1996).

[46] E. A. Fadlun, R. Verzicco, P. Orlandi, and J. Mohd-Yusof, Combined immersed-boundary finite-difference methods for three-dimensional complex flow simulations, J. Comput. Phys. **161**, 35 (2000).

[47] J. Yang and E. Balaras, An embedded-boundary formulation for large-eddy simulation of turbulent flows interacting with moving boundaries, J. Comput. Phys. **215**, 12 (2006).

[48] E. P. van der Poel, R. Ostilla-Mónico, J. Donners, and R. Verzicco, A pencil distributed finite difference code for strongly turbulent wall–bounded flows, Computers & Fluids **116**, 10 (2015).

[49] R. Ostilla-Mónico, R. Verzicco, and D. Lohse, Effects of the computational domain size on direct numerical simulations of Taylor-Couette turbulence with stationary outer cylinder, Phys. Fluids **27**, 025110 (2015).

[50] X. Zhu, R. Ostilla-Monico, R. Verzicco, and D. Lohse, Direct numerical simulation of Taylor-Couette flow with grooved walls: torque scaling and flow structure, J. Fluid Mech. **794**, 746 (2016).

[51] M. Avila, Stability and Angular-Momentum Transport of Fluid Flows between Co-rotating Cylinders, Phys. Rev. Lett. **108**, 124501 (2012).

[52] L. D. Landau and E. M. Lifshitz, Fluid Mechanics (Pergamon Press, Oxford, 1987).

Acknowledgements

We gratefully acknowledge V. Mathai for insightful discussions. We would like to thank G. W. Bruggert and M. Bos, as well as G. Mentink and R. Nauta for their technical support and D.P.M. van Gils and R. Ezeta for various discussions and help with the experiments. The work is financially supported by the Dutch Foundation for Fundamental Research on Matter (FOM), the Netherlands Center for Multiscale Catalytic Energy Conversion (MCEC), the Dutch Technology Foundation (STW) and a VIDI grant (No. 13477), all sponsored by the Netherlands Organisation for Scientific Research (NWO). We thank the Dutch Supercomputing Consortium SurfSARA, the Italian supercomputer FERMI-CINECA through the PRACE Project No. 2015133124 and the ARCHER UK National Supercomputing Service through the DECI Project 13DECI0246 for the allocation of computing time.

Author Contributions X.Z., S.G.H., R.A.V., R.V., C.S. and D.L. conceived the idea. R.A.V. and D.B. performed the measurements. X.Z. performed the numerical simulations. X.Z. and R.A.V. analyzed the data. X.Z., R.A.V. and D.L. wrote the paper. R.V., C.S. and D.L. supervised the project. All authors discussed the physics and proofread the paper.

Author Information Reprints and permissions information is available at www.nature.com/reprints. The authors declare no competing financial interests. Readers are welcome to comment on the online version of the paper. Correspondence and requests for materials should be addressed to D.L. (d.lohse@utwente.nl) or C.S. (chaosun@tsinghua.edu.cn).